Journal of Industrial and Engineering Chemistry 98 (2021) 308–317

Contents lists available at ScienceDirect

Journal of Industrial and Engineering Chemistry

journal homepage: www.elsevier.com/locate/jiec

Biowaste-originated heteroatom-doped porous carbonaceous material for electrochemical energy storage application☆

Raji Atchudan[a,*,1], Thomas Nesakumar Jebakumar Immanuel Edison[a,1], Mani Shanmugam[b,1], Suguna Perumal[a,1], Rajangam Vinodh[c,1], Thirunavukkarasu Somanathan[d,1], Yong Rok Lee[a,*]

[a] School of Chemical Engineering, Yeungnam University, Gyeongsan 38541, Republic of Korea
[b] Department of Science and Humanities, Institute of Aeronautical Engineering, Dundigal, Hyderabad 500043, India
[c] School of Electrical and Computer Engineering, Pusan National University, Busan 46241, Republic of Korea
[d] Department of Chemistry, School of Basic Sciences, Vels Institute of Science, Technology & Advanced Studies (VISTAS), Chennai 600117, India

ARTICLE INFO

Article history:
Received 2 September 2020
Received in revised form 8 December 2020
Accepted 22 March 2021
Available online 27 March 2021

Keywords:
Biowaste
Carbonization
Heteroatom-doped carbon
Carbonaceous materials
Supercapacitor
Clean energy

ABSTRACT

Here, a unique heteroatom-doped spongy carbonaceous material from dwarf banana peel has been synthesized successfully using the one-step hydrothermal method. The discarded banana peel was reused as a carbon source for the formation of heteroatom-doped porous carbon. This biowaste-derived heteroatom-doped porous carbonaceous material (BH-PCM) has plenty of interconnected pores with an acceptable surface area of 213 $m^2 g^{-1}$. Thoroughly characterized BH-PCM has been used as electrode material for supercapacitor using a three-electrode system with an aqueous 1 M H_2SO_4 solution. The as-synthesized BH-PCM holds an excellent specific capacitance of 137 $F g^{-1}$ at 0.5 $A g^{-1}$ and an impressive rate performance with a capacitance enduring 51 $F g^{-1}$ at 5.0 $A g^{-1}$. After 10,000 galvanostatic charge–discharge cycles, an initial capacitance of 94% was maintained. To show the practical applicability of the BH-PCM, the symmetrical two-electrode cell was fabricated and delivered the gravimetric specific capacitances of 87 $F g^{-1}$ at 1 $A g^{-1}$. The excellent electrochemical performance of BH-PCM towards supercapacitor was due to their high surface area, reasonable heteroatom doping rate, and a suitable degree of graphitization. This study offers a green approach for the development of environmental-friendly potential carbon-based electrode, by converting biowaste to clean/green energy.

Introduction

We are in urgent indeed of portable high-performance energy-storage devices because of the energy crisis and environmental pollution [1–4]. Among the energy-storage devices, supercapacitors have attracted researchers because of their outstanding properties including high power density, fast charge–discharge, prolonged cycle stability life, safety, and environmentally friendly [5–9]. Usually, supercapacitors are classified as pseudocapacitors and electrochemical double-layer capacitors (EDLCs) through their energy-storage mechanisms [10–12]. Electrode materials are one of the most important components for the supercapacitors that affect performance and large-scale applications. Hence, the researcher focusing the appropriate electrode materials for the high-performance supercapacitors. Generally, transition metal oxides, conducting polymeric materials, and carbonaceous materials were used as electrode materials [13]. At present, in supercapacitors, carbonaceous materials such as fullerenes, carbon nanotubes, graphene, carbon nanofibers, carbon aerogels, and porous carbon are widely used as electrode materials [14,15]. While they have unique features such as inexpensive, abundant in nature, high surface area, enrich in pore structure, easy surface modification, excellent chemical stability, and the operating mechanism of EDLC [16–21]. In the EDLC mechanism, the specific capacitance (C_s) value of the supercapacitor is controlled by the charges stored at the surface of the electrode material [22,23]. Carbonaceous materials with high surface areas showed high capacity at the electrode-electrolyte

☆ Supporting information: materials, instrumentation methods, fabrication of working electrode, electrochemical measurements, XRD pattern, XPS survey spectrum, surface area analysis, and electrochemical performance of the synthesized BH-PCM.

* Corresponding authors.
E-mail addresses: atchudanr@yu.ac.kr (A. Raji), yrlee@yu.ac.kr (Y.R. Lee).

[1] Authors contributed equally to this work.

https://doi.org/10.1016/j.jiec.2021.03.037
1226-086X/

interfaces [24]. Among the various carbonaceous materials mentioned above, carbonaceous materials derived from the biowaste/biomass attained great attention among researchers. Biowaste is renewable and is the most abundant resource on the earth. Further, they are cost-effective and are environmentally friendly as compared to coal and petroleum-derived carbon materials [3,25–30]. But, these carbon-based supercapacitors endure lower energy-storage and rate capability. Thus the widespread research works have shown that the performances of energy-storage for carbonaceous materials derived from biomass are strongly leaned on their structures [31]. The porous materials show promising results and therefore, biowaste/biomass-derived porous carbonaceous materials may be an option to achieve effective surface area, for heteroatom doping, and surface/structure morphology for high energy-storage devices [32].

Herein, we have developed heteroatom-doped porous carbonaceous material from the waste banana peel (biowaste) by the carbonization method. The resulting biowaste-derived heteroatom-doped porous carbonaceous material (BH-PCM) has been thoroughly characterized using nitrogen physisorption isotherms, field emission scanning electron microscopy (FESEM) with energy-dispersive X-ray spectroscopy (EDS), transmission electron microscopy (TEM), High-resolution TEM (HRTEM), X-ray photoelectron spectroscopy (XPS), attenuated total reflectance Fourier transform infrared (ATR-FTIR) spectroscopy, Raman spectroscopy, and X-ray diffraction (XRD) techniques. This novel BH-PCM was employed as an active electrode material for supercapacitors which showed an outstanding electrochemical double-layer capacitance (EDLC) with prolonged cycling stability. Promising electrochemical performances of the BH-PCM were owing to the doping of heteroatom (nitrogen and oxygen) and the large surface area of BH-PCM with mesoporous nature. The present work has been compared with recent reports about carbon-based materials for supercapacitors to determine the superiority of the synthesized BH-PCM. Moreover, this work proposes an economical and simple method to transform the biowaste into a heteroatom-doped porous carbon composite for environmentally friendly energy-storage applications.

Experimental

Synthesis of BH-PCM

Dwarf banana peels were collected in wet-condition (food-waste/biowaste) and cut into small pieces subsequently, dried at room temperature for 2 days (48 h) under ambient condition. In a simple horizontal tubular furnace gas flow control units, dried waste banana peels were charred in the argon atmosphere at 800 °C for 2 h. In a typical growth experiment, ca. 5 g dried waste banana peel was placed in a quartz boat inside a quartz tube (Length and diameter of the tube are around 1000 mm and 60 mm, respectively). The dried waste banana peel was purged by argon with a flow rate of 200 mL min^{-1} up to 800 °C with a ramp rate of 5 °C min^{-1} and then maintained at 800 °C for 2 h to carbonize the reactant (dried waste banana peel). Subsequently, the furnace was allowed to cool to room temperature under the argon atmosphere. The obtained black carbon flakes were well-grounded using agate mortar and pestle to make a homogeneous fine powder. Further, the synthesized BH-PCM was examined thoroughly by numerous physicochemical characterization techniques (Kindly refer to supporting information for the instrumentation detailed description). Scheme 1 shows the illustration of the detailed synthesis procedure of the BH-PCM from the dwarf banana peel through a simple one-step carbonization method.

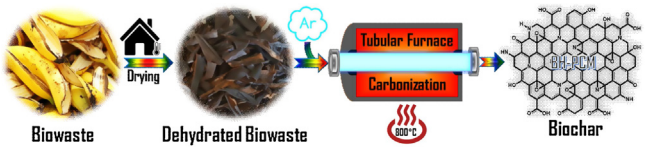

Scheme 1. Illustrate the formation of BH-PCM from the dwarf banana peel through a simple one-step carbonization method.

Results and discussion

Physicochemical characterization of BH-PCM

The morphology of BH-PCM from dwarf banana peel was illustrated by FESEM. The FESEM images with different magnifications of the BH-PCM (Fig. 1(a–i)) showed a three-dimensional aerogel network structure of smooth surface with disordered pores. Such pore structures are favorable for the successive electrochemical applications due to the high internal permeability of electrolytes into the porous structure of BH-PCM. Fig. 2(a–e) displays the FESEM images and the corresponding elemental mapping of the BH-PCM. Fig. 2(b–e) reveals the elemental mapping images of BH-PCM with carbon, oxygen, potassium, and nitrogen elements. The oxygen, nitrogen, and potassium were distributed evenly in the carbon framework. Fig. 2(f) depicts the EDS analysis which further confirms the elemental composition of BH-PCM. Also, the morphology of the BH-PCM was confirmed by TEM and HRTEM measurements. In Fig. 3(a–c), TEM images of BH-PCM displayed the disordered porous structure which contains several interconnected mesopores and micropores. These abundant micropores and mesopores in the BH-PCM material from the dwarf banana peel are expected to give enough space for quick access of electrolyte. Also shorten the pathways for ions to diffuse from the mesopores to the micropores [33,34]. The HRTEM images of BH-PCM (Fig. 3(d–f)) confirm the lattice fringes at the edge of the porous carbon which means the acceptable degree of graphitization of BH-PCM and thus improves the electrical conductivity.

Generally, XRD analysis is used to confirm the degree of graphitization and the crystallinity of carbon-based materials. XRD pattern of the synthesized BH-PCM is shown in Fig. S1. There are four diffraction peaks around 25, 42, 44 and 54° corresponds to the sp^2-hybridization of carbon (002), (100), (101), and (004) planes, respectively which are nearly close to the typical graphite/graphene patterns (JCPDS Card No.: 41-1487) [35–38]. The sp^2-hybridization of carbon (002) planes of BH-PCM slightly shifted towards lower 2θ values, suggesting a slight amorphous nature of BH-PCM. In addition, the peaks around 28.5, 40.6, 50.3, 58.7, 66.4, and 73.8° are corresponding to the potassium elements [39]. The peak intensity of potassium phases is higher than that of carbon phases due to high crystallinity and doping of potassium in the carbon structure. This supports the moderate crystallinity of the synthesized BH-PCM. Compared with high crystalline materials, materials with reasonable crystallinity lead to extra transportation channels which improve the electrochemical performance [40]. Further characterization of the degree of graphitization and the structural defects of BH-PCM was determined by Raman spectroscopy. As illustrated in Fig. 4(a), the BH-PCM exhibits two prominent Raman peaks locating at 1345 cm^{-1} (D-band) and 1590 (G-band) which are assigned to the typical graphitic carbonaceous materials [41–43]. The intense D-band is responsible for the disordered carbon (sp^3) sites on the graphitic carbon planes [44]. G-band is generated by the tensile movement of all sp^2 hybridization carbons in the aromatic rings. The intensity ratio of the D- to G-band (I_D/I_G) is advised about the disorder quantity of the carbon materials [45]. The I_D/I_G value of the BH-PCM is slightly greater than one (1.1), reflects the defects of BH-PCM. The defects

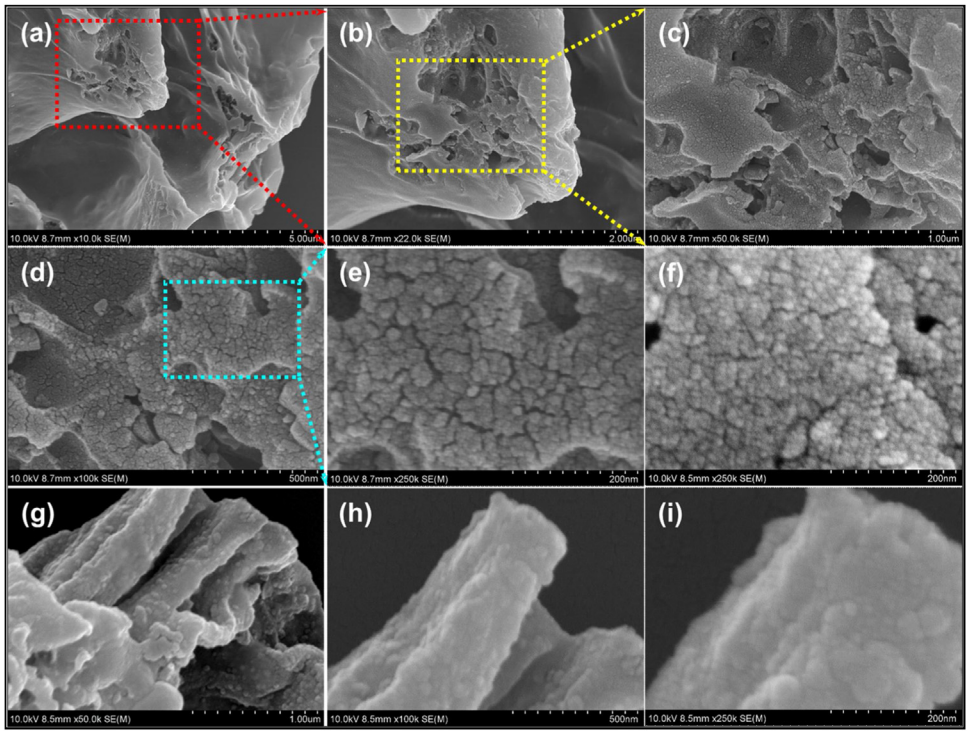

Fig. 1. (a–i) FESEM images with different magnifications of synthesized BH-PCM.

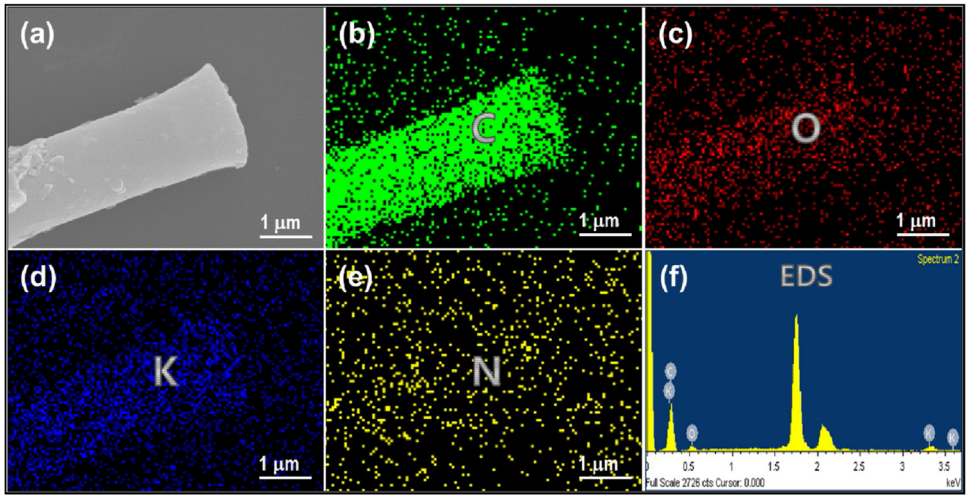

Fig. 2. (a) FESEM image, and corresponding elemental mapping of (b) carbon, (c) oxygen, (d) potassium, and (e) nitrogen for the synthesized BH-PCM. (f) EDS spectrum of synthesized BH-PCM.

are due to the doping of heteroatoms over the porous carbon structure [46,47]. However, these heteroatoms enhance the electrochemical performances of the prepared BH-PCM. In addition, the area of D-band to G-band is considered as the disorder degree of the carbon material, typically expressed as A_D/A_G. The obtained peaks in the region of 1000–2000 cm^{-1} were deconvoluted to determine the comparative content of the area of D-band (disordered part) to the area of G-band (ordered part) in the BH-PCM and presented as inset Fig. 4(a). The large area of D-band compared to G-band suggesting a moderate degree of graphitization. XRD and Raman results suggest the moderate graphitic nature of the prepared BH-PCM.

ATR-FTIR spectroscopy was used to determine the functional groups present in the BH-PCM. As shown in Fig. 4(b), the peak at 3346 cm^{-1} is ascribed to the stretching vibration band of the —OH group, which might be due to the physically adsorbed H_2O molecules or —OH groups originate from the phenolic structure over the synthesized materials. The absorption peaks at around 3267 and 2924 cm^{-1} were assigned to the N—H stretching and asymmetric C—H stretching vibration bands, respectively [48,49]. The shoulder peak at 1650 cm^{-1} is an indication of the presence of undissociated carbonyl groups [50]. The absorption peaks at 1580 and 1510 cm^{-1} were ascribed for the C=C and C—N/N—H bonds, respectively [37,51]. The vibration peaks at 1380 and 1220 cm^{-1} are accredited to the bending band of the C—H and C—OH groups, respectively. A strong band at 995 cm^{-1} and a shoulder band at 1083 cm^{-1} were caused by the functional group of C—O—C epoxy groups in the aromatic carbon rings [52,53]. The absorption peaks

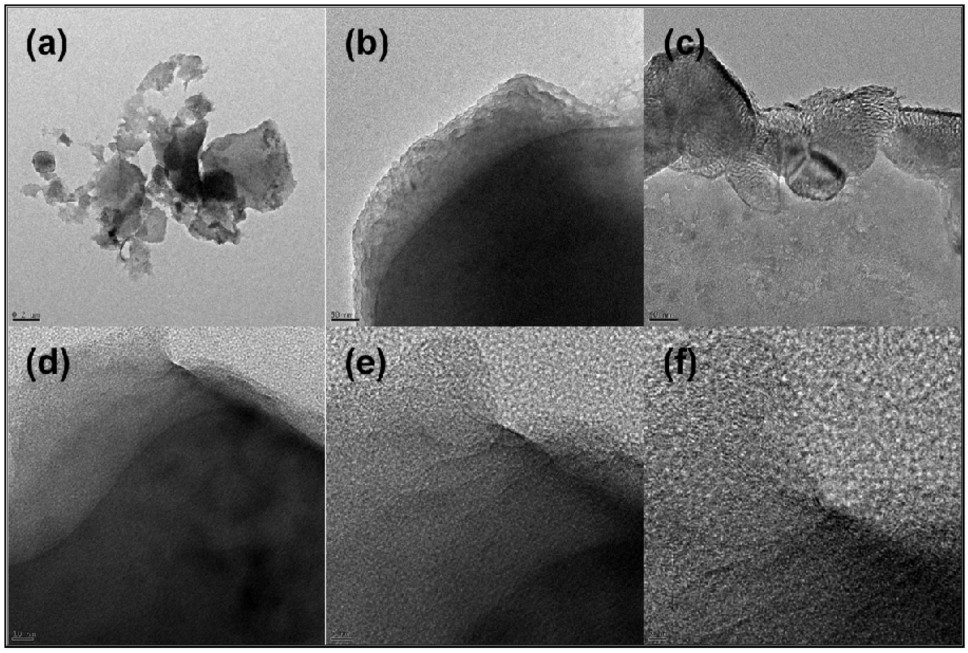

Fig. 3. (a–c) TEM images and (d–f) HRTEM images with different magnifications of the synthesized BH-PCM.

at 820 and 695 cm^{-1} are due to the strong wagging of the hydrogen atoms in the aromatic ring with a=C—H/CH=CH groups [48]. ATR-FTIR spectrum indicates the presence of nitrogen- and oxygen-containing functional groups in BH-PCM. This shows a consistent result with the EDS result. XPS spectroscopy is a powerful technique to understand and to quantify the chemical composition of the BH-PCM. As shown in the XPS survey spectrum (Fig. S2), the BH-PCM has carbon, nitrogen, oxygen, and potassium atoms which confirm the presence of heteroatoms in the prepared BH-PCM structure. Fig. 4(c) represents the deconvolution spectra of C 1s peak which showed five peaks at 284.5, 285.4, 286.4, 288.1, and 289.1 eV corresponding to the C—H (hydrogen-bonded carbon rings)/C=C (sp^2 aromatic rings)/C—C (sp^3 hybridized carbon), the oxygen-based functional groups, such as C—OH/C—N—C (hydroxyl group/nitrogen singly bonded to aromatic carbon), C—O—C (oxygen singly bonded to aromatic carbon), C=O/C=N (oxygen/nitrogen doubly bonded to aromatic carbon), and HO—C=O (oxygen singly and doubly bonded to aromatic carbon), respectively [54–56]. Deconvolution of the K 2p peak (Fig. 4(d)) revealed two peaks appeared at 293.3 and 296.1 eV corresponding to K $2p_{3/2}$ and K $2p_{1/2}$, respectively. The high-resolution N 1s spectrum (Fig. 4(e)) of BH-PCM was deconvoluted into three individual peaks appeared at 398.2, 399.8 and 401.7 eV corresponds to C—N—C, C—N—H and $(C)_3$—N bonds, respectively, confirm the presence of nitrogen moieties over the carbon framework [57–59]. Deconvolution of the O 1s peaks (Fig. 4(f)) result in three peaks which are responsible for the oxygen functionalities such as C=O/C—OH (531.2 eV), C—O—C (532.5 eV), and OH—C=O (533.8 eV) groups on the surface of the BH-PCM [60–62]. ATR-FTIR, EDS, elemental mapping, XRD, Raman, and XPS analyses confirm the existence of heteroatoms on the surface of the BH-PCM.

The porous nature including specific surface area and pore diameter of BH-PCM material was determined by nitrogen physisorption study. Nitrogen physisorption isotherms (adsorption–desorption) and the pore size spreading graph of the BH-PCM are shown in Fig. S3. The steep uptakes of nitrogen at the lower relative pressure ($P/P_0 < 0.1$) were ascribed to micropores and mesoporous in BH-PCM. In addition, a small hysteresis loop in the higher relative pressure ($P/P_0 > 0.9$), representing the existence of a smaller amount of macrospores which might originate from the voids between the mesoporous carbon entities. According to the IUPAC classification, the overall isotherms of BH-PCM belonged to the typical IV-type with the mixture of H1 and H3-type hysteresis loops [63]. The Brunauer–Emmett–Teller (BET) specific surface area of the BH-PCM was calculated to be 213 $m^2 g^{-1}$ from the nitrogen adsorption isotherm. Further, the pore size distribution (Fig. S3(b)) of the BH-PCM was obtained through the Barrett–Joyner–Halenda (BJH) method. The pore sizes of the BH-PCM were below 10 nm. The presence of major mesopores affords a large surface area for the active materials/molecules to quickly penetrate the electrolyte. From the BET measurement and pore size distribution analysis, the BH-PCM is estimated to progress the ion transportation for the proficient redox reactions and meet the requirement for supercapacitor applications [64].

Electrochemical behavior of BH-PCM

The synthesized BH-PCM with heteroatoms (nitrogen and oxygen)-doped enhances the surface wettability, gives more active sites, mesopore structure, and provides high surface area. These are more favorable for larger mass loading and electrolyte transport. In addition, the heteroatom improves electron transport in the BH-PCM during the electrochemical reaction. All these characteristics will pave the way for the improvement of electrochemical properties. Hence, the electrochemical performance of the BH-PCM was examined by cyclic voltammetry (CV), galvanostatic charge–discharge (GCD), and electrochemical impedance spectroscopy (EIS) measurements using a three-electrode configuration with 1 M H_2SO_4, and the outcome is displayed as Fig. 5. The CV curves of BH-PCM at different scan rates from 5 to 100 mV s^{-1} with voltages between −0.1 and 0.6 V as shown in Fig. 5(a). All the CV curves display a relatively symmetric rectangular shape and display a good current response, signifying the BH-PCM owns the energy-storage mechanism of electrochemical double-layer capacitance (EDLC) behavior. The physical phenomena of electrostatic storage occurring at the electrode-electrolyte interface. The nearly rectangular shape of CV also suggesting reversible electrochemical performance. The distortion

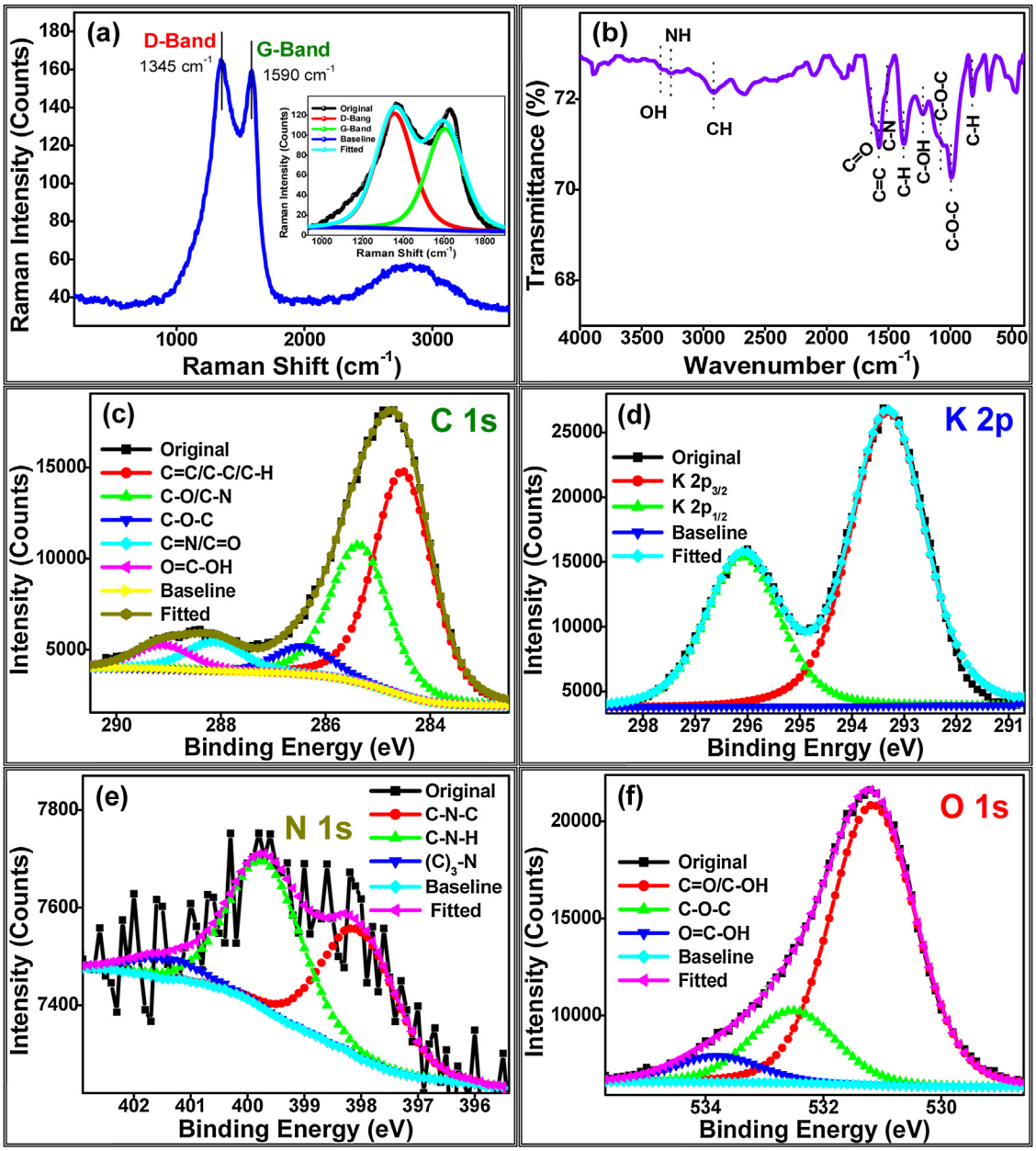

Fig. 4. (a) Raman spectrum and (b) ATR-FTIR spectrum of the synthesized BH-PCM. XPS high-resolution spectra of (c) C 1s, (d) K 2p, (e) N 1s, and (f) O 1s for the synthesized BH-PCM.

of the CV curves has no noticeable difference even at a higher scanning rate (Fig. S4), demonstrating that the system of electrodes has lower resistance and a more desirable electrochemical behavior [65]. Fig. 5(b) shows the GCD curves of BH-PCM between −0.1 and 0.6 V at various current densities (CUDs) from 0.5 to 5 A g^{-1}. In correspondence with CV curves, the BH-PCM is close to the shape of an isosceles triangle which owing to the idyllic EDLC behavior of electroactive material. EDLC depends on the rapid and reversible ion adsorption–desorption process without limitation by the electrochemical kinetics, which eventually leads to forming EDLC as illustrated in the inset of Fig. 5(e). The C_s of the BH-PCM were calculated (refer to equation (S1) in Supplementary information) to be 137, 112, 85, 69, 57, and 51 F g^{-1} at the various CUDs of 0.5, 1.0, 2.0, 3.0, 4.0, and 5.0 A g^{-1}, respectively. The relationship between C_s and CUD of samples is revealed by the GCD test in the range of 0.5–5.0 A g^{-1} as summarized in Fig. 5(c). The C_s of BH-PCM gradually decreased with increasing CUDs but it retains 38% suggesting that the synthesized BH-PCM having acceptable capacitance retentions. Moreover, the BH-PCM possesses outstanding capacitive performance even at high CUD. This excellent performance of BH-PCM is because of its acceptable degree of graphitization, and wettable surface (the wettable surface obtained due to the doping of heteroatom), which ensures that the electrolyte ions have sufficient time to distribute into the greatly established microporous/mesoporous structure. To show the greater activity of the synthesized BH-PCM, the obtained values were compared with the reports related to carbonaceous materials (Table 1 [5,18,29,63,66–70]). The present work (synthesized BH-PCM) displays favorably higher C_s value with prolonged stability than the other carbonaceous materials. The excellent electrochemical performances of synthesized BH-PCM are might due to the electrochemically stable carbon structure of BH-PCM.

Further, the EIS study was performed to determine the electrochemical behavior of the BH-PCM and was used to test

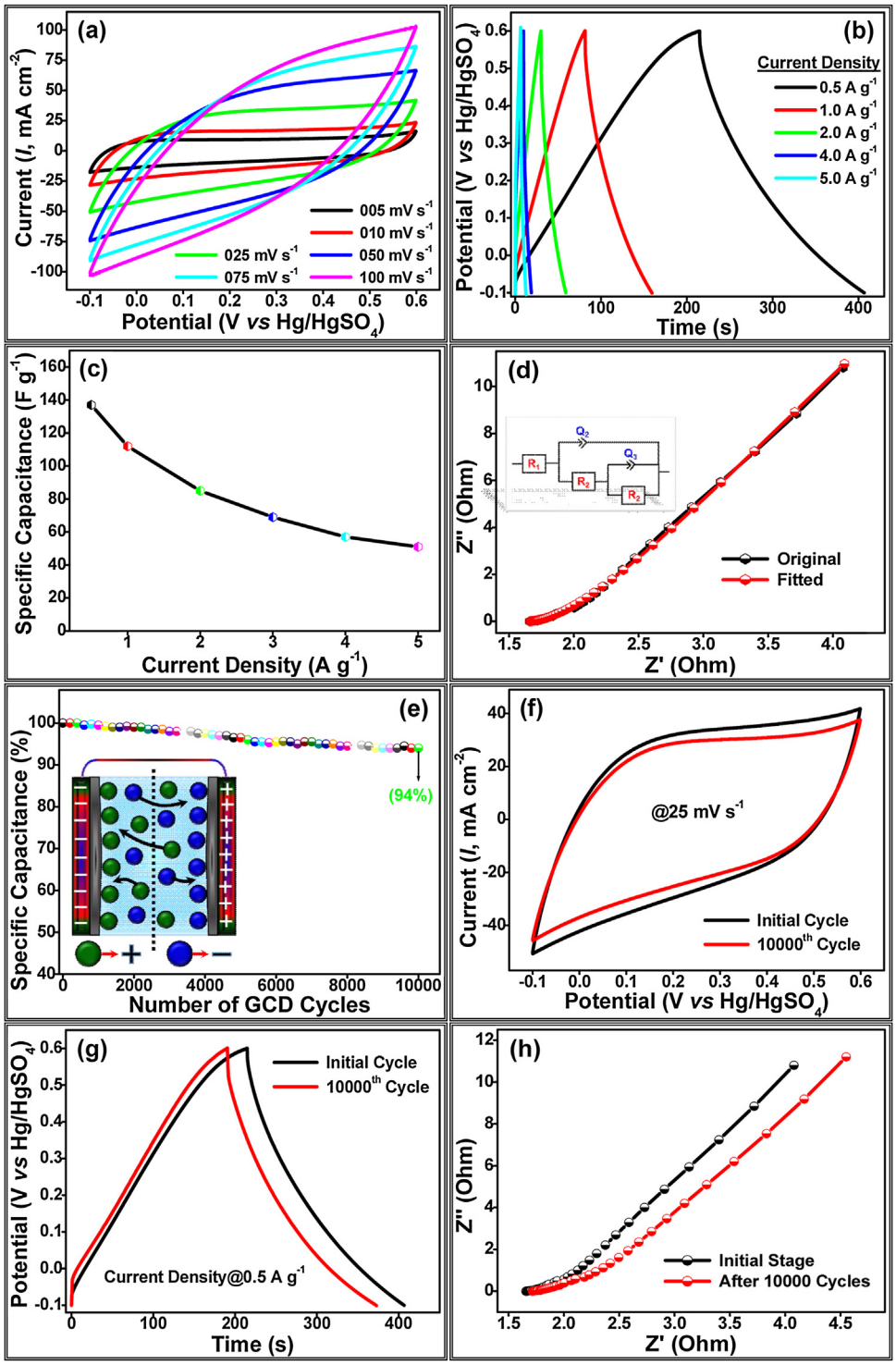

Fig. 5. (a) CV curves at various scan rates and (b) GCD curves at various CUDs of the synthesized BH-PCM. (c) CUD-dependent C_s, (d) EIS spectrum with a fitted equivalent circuit, and (e) prolong stability up to 10,000 cycles of synthesized BH-PCM. (f) CV curves, (g) GCD curves, and (h) Nyquist plots of the synthesized BH-PCM before and after 10,000 cycles.

the resistance of the supercapacitors. The impedances result of BH-PCM in 1 M H_2SO_4 electrolyte in the frequency range of 0.01–100,000 Hz is presented in Fig. 5(d). Nyquist plots (EIS) of BH-PCM contain two different times constant, a small distorted semicircle at high-frequency regions that correspond to the charge transfer resistance (R_{ct}) at interfaces and this reveals the kinetics of electrochemical reaction necessarily [71]. Then, a slanting/almost vertical (inclined) line at a low-frequency region corresponds to the ion-diffusion resistance in the electrolyte and the mass capacitance with leakage resistance in parallel combination [11]. The EIS is fitted using an equivalent circuit of $R_1 + Q_2/R_2 + Q_3/R_3$ by Z-View software and their equivalent electric circuit is displayed in the inset of Fig. 5(d). The solution resistance (R_1, 1.661 $\Omega\,cm^{-2}$), charge–transfer resistance (R_2, 2.517 $\Omega\,cm^{-2}$), and the coating resistance (R_3, 791 $\Omega\,cm^{-2}$) are calculated from the fitted Nyquist plots. The capacitances including Q_2 and Q_3 of BH-PCM are

Table 1
Comparison of present work with the previously reported literature on biomass carbon-based composites for supercapacitors.

Electrode materials	Aqueous electrolyte	Synthesis method	C_s ($F g^{-1}$)/CD ($A g^{-1}$)	Cycle/retention (%)	Reference
N-CS	1 M H_2SO_4	Carbonization	191.9/0.1	10,000/110	[66]
N-Py-700	1 M H_2SO_4	Carbonization	374/0.1	15,000/96	[67]
N-GCSs	1 M H_2SO_4	Hydrothermal	70/0.5	2000/120	[68]
NR	1 M Na_2SO_4	Carbonization	137/0.5	5000/82	[5]
PAN/PVDF	6 M KOH	Carbonization	265/0.05	2000/81	[18]
HPI	6 M KOH	Carbonization	211.3/0.5	10,000/99.9	[63]
HSCCA	6 M KOH	Carbonization	148.6/0.25	–	[69]
N-CNG	1 M H_2SO_4	Carbonization	81/0.5	10,000/95	[70]
WS-AC	1 M H_2SO_4	Carbonization	110/0.5	1000/180	[29]
BH-PCM	1 M H_2SO_4	Carbonization	137/0.5	10,000/94	This work

calculated as 2.361 and 1.232 F cm^{-2}, respectively. The cycle stability of the BH-PCM is shown in Fig. 5(e), The GCD cycles were performed up to 10,000 cycles at 5 A g^{-1}, and the C_s retention rate was as high as 94% after 10,000 cycles, which confirmed the extremely high GCD cycle strength of this material and great potential for employment as a supercapacitor. The CV, GCD, and EIS analyses were conducted after prolonged stability of BH-PCM and compared to initial studies and corresponding results are shown in Fig. 5(f), (g), and (h), respectively. After prolonged stability of the CV, GCD, and EIS curves nearly similar to that of initial curves of the CV, GCD, and EIS suggesting the BH-PCM possess excellent stability towards supercapacitor performance in 1 M H_2SO_4 solution. Overall, the BH-PCM had a high surface area with a vast number of mesopores which could accelerate ion transportations into inner channels of pore and afford abundant surface regions for ion accruals. The surface heteroatoms including nitrogen and oxygen in the BH-PCM are responsible to increase C_s.

To show the practical applicability of the synthesized BH-PCM, the symmetrical two-electrode cell was fabricated using the synthesized BH-PCM over carbon cloth. The fabricated two-electrode cell was examined by CV and GCD measurements in a 1 M aqueous H_2SO_4 solution. Fig. 6(a) displays the CV curves of the two-electrode cell at different scan rates (5–100 mV s^{-1}) with the potential window of 0–1.5 V. It is obvious that all the CV curves nearly rectangular shapes without any redox-peaks, which confirm the double layer ideal capacitive response of BH-PCM in 1 M aqueous H_2SO_4 solution. Noticeably, well rectangular shapes were observed at a slow scan rate (<50 mV s^{-1}) compared to a fast scan rate (>50 mV s^{-1}). This is because, at a slow scan rate, a vast number of electrolyte ions access the electrode surface. Besides, the total current area of the CV curves is gradually increased from 5 to 300 mV s^{-1} (Fig. S5 and Fig. 6(a)). Fig. 6(b) represents the GCD curves of the synthesized BH-PCM at different CUDs from 1 to 5 A g^{-1} in a two-electrode system. The figure shows near triangular-shaped GCD curves, which demonstrate the linear dependence of stored charge under the applied potential window. This result revealed that the charge storage behavior of the fabricated two-electrode system is completely based on the electrostatic accumulation of ions present in the electrolyte on the porous double-layer structures of the electroactive BH-PCM. The calculated gravimetric specific capacitances (C_{gs}) of electroactive BH-PCM is around 87, 66, 56, 50, and 40 F g^{-1} at the applied CUDs of 1, 2, 3, 4, and 5 A g^{-1}, respectively (Fig. 6(c)) using the equation (S2) (Kindly refer the Supporting information). Based on C_{gs}, the energy density

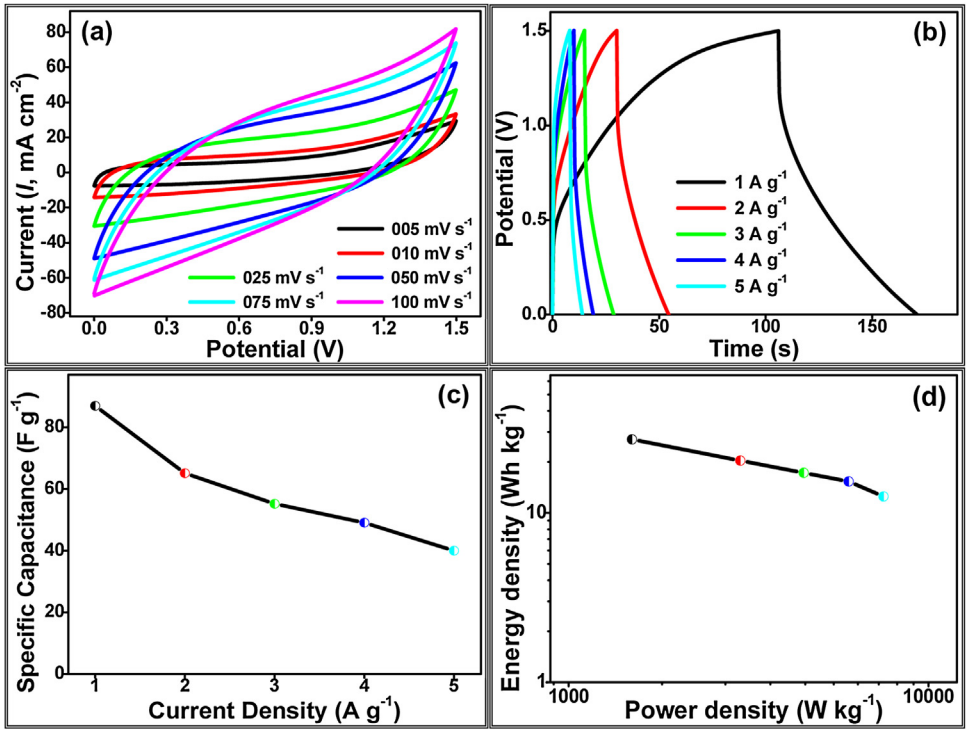

Fig. 6. (a) CV curves at different scan rates and (b) GCD curves at different CUDs of the synthesized BH-PCM. (c) C_{gs} at different CUDs, and (d) Ragone plots (E_D vs P_D) of the synthesized BH-PCM.

(E_D) and power density (P_D) of the synthesized electroactive BH-PCM were calculated as 27.17, 20.35, 17.25, 15.34, 12.5 Wh kg^{-1} and 1500, 3000, 4500, 6000, and 7500 W kg^{-1}, respectively using the equations (S3) and (S4) (Kindly refer the Supporting information) and the results presented in Ragone plots as Fig. 6(d). The two-electrode studies revealed that the synthesized electroactive BH-PCM can be applied as the symmetric electrode for supercapacitor devices. These excellent electrochemical properties of the synthesized electroactive BH-PCM is due to the porous structure with an acceptable graphitic nature.

The structural morphology of the bare conducting substrate (carbon cloth-CC) and BH-PCM coated conducting substrate were analyzed by FESEM. The FESEM images of the BH-PCM coated conducting substrate (working electrode) before and after the electrochemical performance (the GCD, CV, and EIS analyses) were compared to determine the structural strength of the prepared BH-PCM (Fig. 7). Fig. 7(a–c) displays the FESEM images of bare CC which reveals the twill weave structure in the low magnification. Besides, in the high magnification images, the carbon fibers were smooth surface (Fig. 7(a–c)) [72]. The BH-PCM is evenly distributed

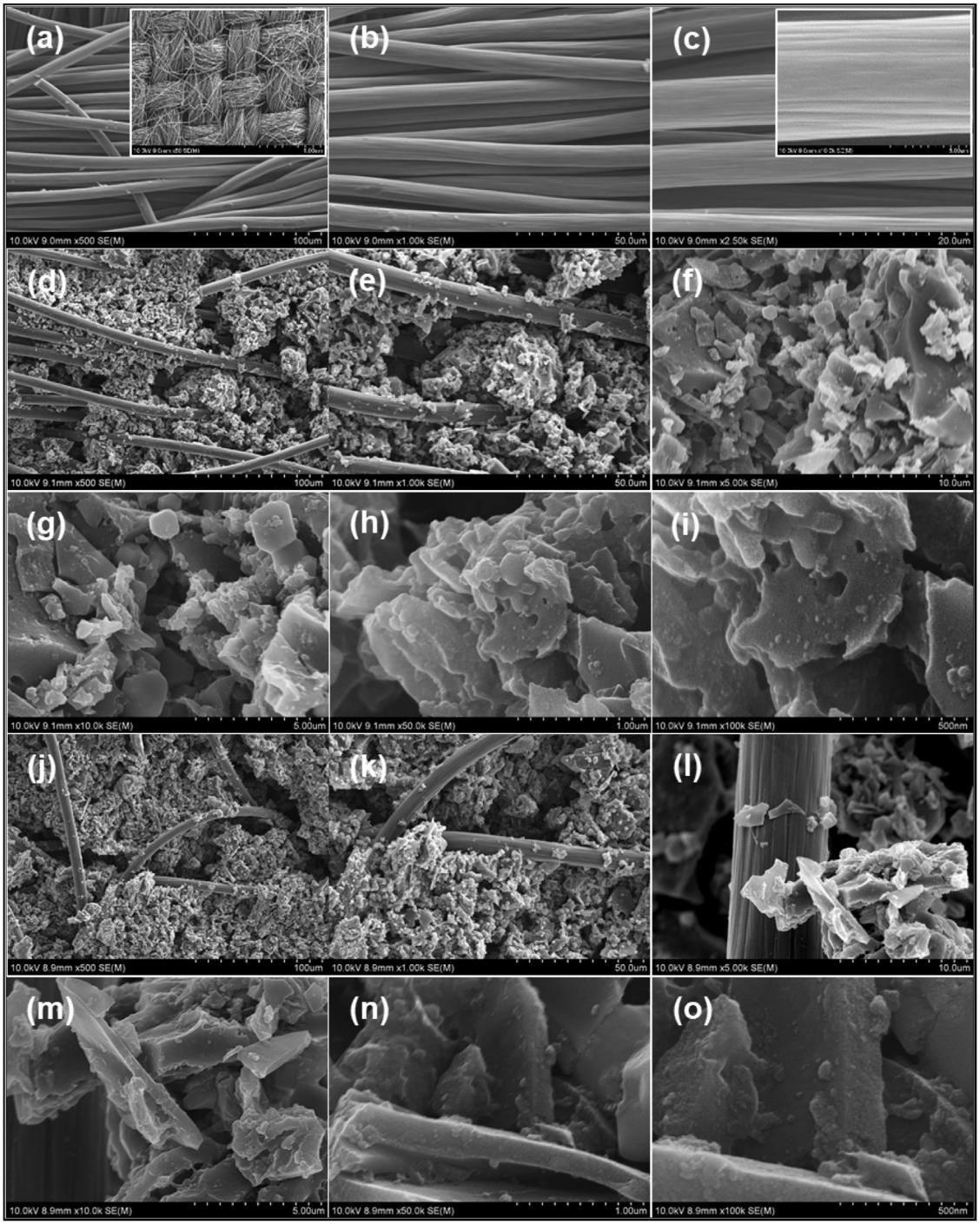

Fig. 7. (a–c) FESEM images of the bare CC, (d–i) FESEM images of the BH-PCM coated CC before the electrochemical performance, and (j–o) FESEM images of the BH-PCM coated CC after the electrochemical performance.

on the CC before the electrochemical measurements (Fig. 7(d–i)). After all the electrochemical measurements, the BH-PCM (Fig. 7 (j–o)) displays that there is no noticeable collapse including structural changes and detachment of the BH-PCM from the CC substrate. The images confirm the electroactive BH-PCM coated very well on the conducting substrate. Interestingly, porous smooth morphology retained well even after all the electrochemical studies including prolonging stability up to 10,000 GCD cycles. Thus, the synthesized BH-PCM is suitable for electrochemical energy-storage applications.

Conclusions

A novel BH-PCM was synthesized successfully from waste dwarf banana peel by the facile one-step carbonization for energy-storage applications. The structural characterization and chemical composition analysis indicates that the BH-PCM possesses a microporous/mesoporous structure with a reasonable BET surface area, acceptable heteroatom doping, and a suitable degree of graphitization/crystallization. The as-synthesized BH-PCM displays a high C_s of 137 $F g^{-1}$ at the CUD of 0.5 $A g^{-1}$ in an aqueous 1 M H_2SO_4 solution. Excellent C_s retention of 94% was also demonstrated after 10,000 GCD cycles. In order to show the practical applicability of the synthesized BH-PCM, the symmetrical two-electrode cell was fabricated which delivered a high C_{gs} of 87 $F g^{-1}$ at the CUD of 1 $A g^{-1}$ in a two-electrode system. FESEM images of before and after electrochemical measurement suggest the excellent stability of BH-PCM on conducting substrate. Overall results confirmed that the BH-PCM derived from waste banana peel might serve as renewable, economical, and high-performance electroactive material for energy-storage devices (supercapacitors). Moreover, this work demonstrates a successful example of turning discarded bosh into valuable energy-storage material as well as estimated to provide advantageous tipoffs for the disposal of biowaste/biomass and contributes to environmental cleaning.

Conflict of interest

The authors declare that there is no conflict of interest.

Declaration of Competing Interest

The authors report no declarations of interest.

Acknowledgments

This research was supported by the National Research Foundation (NRF) of Korea funded by the Ministry of Education, Science, and Technology (2012M3A7B4049677), the Ministry of Science, Information and Communications Technology (MSIT) (2017R1C1B5076345), and the MSIT (2018R1A2B2004432).

Appendix A. Supplementary data

Supplementary material related to this article can be found, in the online version, at doi:https://doi.org/10.1016/j.jiec.2021.03.037.

References

[1] B. Wang, L. Ji, Y. Yu, N. Wang, J. Wang, J. Zhao, Electrochim. Acta 309 (2019) 34.
[2] N. Zhao, L. Deng, D. Luo, P. Zhang, Appl. Surf. Sci. 526 (2020) 146696.
[3] Z. Li, D. Guo, Y. Liu, H. Wang, L. Wang, Chem. Eng. J. 397 (2020) 125418.
[4] C. Li, X. Zhang, K. Wang, F. Su, C.-M. Chen, F. Liu, Z.-S. Wu, Y. Ma, J. Energy Chem. 54 (2021) 352.
[5] M. Li, J. Yu, X. Wang, Z. Yang, Appl. Surf. Sci. 530 (2020)147230.
[6] S. Kumar, G. Saeed, L. Zhu, K.N. Hui, N.H. Kim, J.H. Lee, Chem. Eng. J. 403 (2021) 126352.
[7] P.-G. Ren, W. He, Z. Dai, X. Hou, F. Ren, Y.-L. Jin, Diamond Relat. Mater. (2020) 108028.
[8] Z. Sui, Z. Chang, X. Xu, Y. Li, X. Zhu, C. Zhao, Q. Chen, Diamond Relat. Mater. 108 (2020)107988.
[9] S. He, W. Chen, Nanoscale 7 (2015) 6957.
[10] Y. Wang, Q. Qu, S. Gao, G. Tang, K. Liu, S. He, C. Huang, Carbon 155 (2019) 706.
[11] J. Zhang, H. Chen, Z. Ma, H. Li, Y. Dong, H. Yang, L. Yang, L. Bai, D. Wei, W. Wang, J. Alloys Compd. 832 (2020)155029.
[12] H. Fan, X. Zhang, Y. Wang, J. Lang, R. Gao, J. Power Sources 474 (2020)228603.
[13] P. Thomas, C.W. Lai, M.R. Bin Johan, J. Anal. Appl. Pyrolysis 140 (2019) 54.
[14] X. Zhou, B. Liu, Y. Chen, L. Guo, G. Wei, Mater. Adv. 1 (2020) 2163.
[15] W. Fan, Y. Shi, W. Gao, Z. Sun, T. Liu, ACS Appl. Nano Mater. 1 (2018) 4435.
[16] G. Yang, S.-J. Park, J. Alloys Compd. 741 (2018) 360.
[17] G. Zhang, T. Guan, N. Wang, J. Wu, J. Wang, J. Qiao, K. Li, Chem. Eng. J. 399 (2020) 125818.
[18] H. Liu, F. Gao, Q. Fan, C. Wei, C. Ma, J. Shi, J. Electroanal. Chem. 873 (2020) 114409.
[19] P. Dai, S. Zhang, H. Liu, L. Yan, X. Gu, L. Li, D. Liu, X. Zhao, Electrochim. Acta 354 (2020)136717.
[20] Y. Wang, X. Gao, Y. Fu, X. Wu, Q. Wang, W. Zhang, C. Luo, Compos. B: Eng. 169 (2019) 221.
[21] D.-M. Xue, S.-C. Qi, X. Liu, Y.-X. Li, X.-Q. Liu, L.-B. Sun, J. Ind. Eng. Chem. 80 (2019) 568.
[22] B. Fang, L. Binder, J. Phys. Chem. B 110 (2006) 7877.
[23] R. Dubey, V. Guruviah, Ionics 25 (2019) 1419.
[24] L.L. Zhang, X.S. Zhao, Chem. Soc. Rev. 38 (2009) 2520.
[25] T. Yumak, G.A. Yakaboylu, O. Oginni, K. Singh, E. Ciftyurek, E.M. Sabolsky, Colloids Surf. A 586 (2020)124150.
[26] B.K. Saikia, S.M. Benoy, M. Bora, J. Tamuly, M. Pandey, D. Bhattacharya, Fuel 282 (2020)118796.
[27] A. Gopalakrishnan, S. Badhulika, Renew. Energy 161 (2020) 173.
[28] S.-Y. Lee, Y. Choi, J.-K. Kim, S.-J. Lee, J.S. Bae, E.D. Jeong, J. Ind. Eng. Chem. 94 (2021) 272.
[29] G.P. Awasthi, D.P. Bhattarai, B. Maharjan, K.-S. Kim, C.H. Park, C.S. Kim, J. Ind. Eng. Chem. 72 (2019) 265.
[30] B. Zhang, D. Yang, X. Qiu, Y. Qian, M. Yan, Q. Li, J. Ind. Eng. Chem. 82 (2020) 220.
[31] F. Yu, S. Li, W. Chen, T. Wu, C. Peng, Energy Environ. Mater. 2 (2019) 55.
[32] B. Zhao, C. Song, F. Wang, W. Zi, H. Du, Microporous Mesoporous Mater. 306 (2020) 110483.
[33] D.-L. Vu, J.-S. Seo, H.-Y. Lee, J.-W. Lee, RSC Adv. 7 (2017) 4144.
[34] Z. Zhou, T. Liu, A.U. Khan, G. Liu, Mol. Syst. Des. Eng. 5 (2020) 153.
[35] R. Atchudan, T.N.J.I. Edison, S. Perumal, R. Vinodh, Y.R. Lee, J. Mol. Liq. 296 (2019)111817.
[36] Z. Liu, D. Tian, F. Shen, P.C. Nnanna, J. Hu, Y. Zeng, G. Yang, J. He, S. Deng, J. Power Sources 458 (2020)228057.
[37] S.-Y. Tsai, R. Muruganantham, S.-H. Tai, B.K. Chang, S.-C. Wu, Y.-L. Chueh, W.-R. Liu, J. Taiwan Inst. Chem. Eng. 97 (2019) 178.
[38] S. Jaworski, M. Wierzbicki, E. Sawosz, A. Jung, G. Gielerak, J. Biernat, H. Jaremek, W. Łojkowski, B. Woźniak, J. Wojnarowicz, L. Stobiński, A. Małolepszy, M. Mazurkiewicz-Pawlicka, M. Łojkowski, N. Kurantowicz, A. Chwalibog, Nanoscale Res. Lett. 13 (2018) 116.
[39] E.-J. Kim, S.-J. Han, J.-H. Wee, J. Korean Soc. Environ. Eng. 37 (2015) 597.
[40] V. Barranco, M.A. Lillo-Rodenas, A. Linares-Solano, A. Oya, F. Pico, J. Ibañez, F. Agullo-Rueda, J.M. Amarilla, J.M. Rojo, J. Phys. Chem. C 114 (2010) 10302.
[41] R. Atchudan, T.N.J. Immanuel Edison, S. Perumal, R. Vinodh, N. Muthuchamy, Y. R. Lee, Fuel 277 (2020)118235.
[42] G. Yuan, H. Li, H. Hu, Y. Xie, Y. Xiao, H. Dong, Y. Liang, Y. Liu, M. Zheng, Electrochim. Acta 326 (2019) 134974.
[43] W.-K. Jo, S. Kumar, M.A. Isaacs, A.F. Lee, S. Karthikeyan, Appl. Catal. B: Environ 201 (2017) 159.
[44] C. Cheng, S. He, C. Zhang, C. Du, W. Chen, Electrochim. Acta 290 (2018) 98.
[45] H. Badenhorst, Sol. Energy 192 (2019) 35.
[46] L. Fan, Z. Li, W. Kang, B. Cheng, Renew. Energy 155 (2020) 309.
[47] H. Zhang, Y. Ling, Y. Peng, J. Zhang, S. Guan, Inorg. Chem. Commun. 115 (2020) 107856.
[48] M. Zhang, H. Yang, Y. Liu, X. Sun, D. Zhang, D. Xue, Nanoscale Res. Lett. 7 (2012) 38.
[49] S. Karthikeyan, D.D. Dionysiou, A.F. Lee, S. Suvitha, P. Maharaja, K. Wilson, G. Sekaran, Catal. Sci. Technol. 6 (2016) 530.
[50] K. Pourreza, N. Bahrami Adeh, N. Mohammadi, J Energy Storage 30 (2020) 101429.
[51] O. Prakash, A. Mungray, S. Chongdar, S.K. Kailasa, A.K. Mungray, J. Environ. Chem. Eng. 8 (2020)102757.
[52] S. Perumal, R. Atchudan, D.H. Yoon, J. Joo, I.W. Cheong, J. Mater. Sci. 55 (2020) 9354.
[53] S.H. Baek, J. Roh, C.Y. Park, M.W. Kim, R. Shi, S.K. Kailasa, T.J. Park, Mater. Sci. Eng.: C 107 (2020)110273.
[54] T.N.J.I. Edison, R. Atchudan, N. Karthik, J. Balaji, D. Xiong, Y.R. Lee, Fuel 280 (2020)118682.
[55] R. Ivan, C. Popescu, A. Pérez del Pino, C. Logofatu, E. György, Appl. Surf. Sci. 509 (2020)145359.
[56] Y. Wang, X. Di, X. Wu, X. Li, J. Alloys Compd. 846 (2020)156215.
[57] R. Atchudan, T.N.J.I. Edison, S. Perumal, N. Muthuchamy, Y.R. Lee, Fuel 275 (2020)117821.

[58] R. Atchudan, T.N.J.I. Edison, K.R. Aseer, S. Perumal, N. Karthik, Y.R. Lee, Biosens. Bioelectron. 99 (2018) 303.
[59] Z. Song, H. Duan, L. Miao, L. Ruhlmann, Y. Lv, W. Xiong, D. Zhu, L. Li, L. Gan, M. Liu, Carbon 168 (2020) 499.
[60] R. Atchudan, N. Muthuchamy, T.N.J.I. Edison, S. Perumal, R. Vinodh, K.H. Park, Y. R. Lee, Biosens. Bioelectron. 126 (2019) 160.
[61] J. Dong, S. Li, Y. Ding, J. Alloys Compd. 845 (2020)155701.
[62] Y. Wang, X. Gao, X. Wu, W. Zhang, C. Luo, P. Liu, Chem. Eng. J. 375 (2019)121942.
[63] Y. Liang, Y. Lu, G. Xiao, J. Zhang, H. Chi, Y. Dong, Appl. Surf. Sci. 529 (2020) 147141.
[64] M. Jin, G. Zhang, F. Yu, W. Li, W. Lu, H. Huang, Phys. Chem. Chem. Phys. 15 (2013) 1601.
[65] S. He, H. Hou, W. Chen, J. Power Sources 280 (2015) 678.
[66] W.-H. Lee, J.H. Moon, ACS Appl. Mater. Interfaces 6 (2014) 13968.
[67] J.-S.M. Lee, M.E. Briggs, C.-C. Hu, A.I. Cooper, Nano Energy 46 (2018) 277.
[68] R. Atchudan, T.N.J.I. Edison, S. Perumal, Y.R. Lee, Appl. Surf. Sci. 393 (2017) 276.
[69] Q. Wang, T. Xia, X. Jia, J. Zhao, Q. Li, C. Ao, X. Deng, X. Zhang, W. Zhang, C. Lu, Carbohydr. Polym. 245 (2020)116554.
[70] R. Atchudan, T.N.J.I. Edison, S. Perumal, P. Thirukumaran, R. Vinodh, Y.R. Lee, J. Taiwan Inst. Chem. Eng. 102 (2019) 475.
[71] X. Zhu, Y. Shang, Y. Lu, C. Liu, Z. Li, Q. Liu, J. Power Sources 471 (2020)228444.
[72] R. Atchudan, T.N.J.I. Edison, S. Perumal, A.S. Parveen, Y.R. Lee, J. Electroanal. Chem. 833 (2019) 357.